Wide-band heterodyne submillimetre wave spectrometer for planetary atmospheres

Erich Schlecht

Jet Propulsion Laboratory, California Institute of Technology
Contact: Erich.Schlecht@jpl.nasa.gov, phone +01-818-354-4887

***Abstract*— We present calculations and measurements on a passive submillimetre wave spectroscopic sounder to gather data on the thermal structure, dynamics and composition of the upper atmosphere of a planet, e.g. the stratosphere of Jupiter, or the entire thickness of the atmosphere of Mars. The instrument will be capable of measuring *wind speeds*, *temperature*, *pressure*, and key constituent *concentrations* in the stratosphere of the target planet.**

This instrument consists of a Schottky diode based front end and a digital back-end spectrometer. It differs from previous space-based spectrometers in its combination of wide tunability (520-590 GHz), and rapid frequency switching between widely spaced lines within that range. This will enable near simultaneous observation of multiple lines, which is critical to the reconstruction of atmospheric pressure and density versus altitude profiles. At the same time frequency accuracy must be high to enable wind speeds to be determined directly by measurement of the line's Doppler shift.

I. Introduction

Recently, NASA and ESA have turned their attention to an Outer Planet Flagship Mission (OPFM) to the Jupiter system, focusing on Ganymede, Europa and other Galilean moons, as well as Jupiter, and to the Saturn system focusing on the Titan. Both studies call for inclusion of a submillimeter spectrometer. The Jupiter measurements will greatly expand on those from the Juno mission currently being built, the prime target being Jupiter's stratosphere. Titan measurements would concentrate on the upper atmosphere dynamics of hydrocarbon chemistry. Another possible target for a submillimetre wave spectrometer is Mars, whose atmosphere is thin enough to be observed all the way to the surface.

Submillimetre spectral observations of these planets' atmospheres will allow multiple physical properties of the atmosphere to be measured as a function of altitude and latitude/longitude:

Concentration of various critical gases of interest
Pressure
Temperature
Wind Velocity

Fig. 1a shows a planet limb sounding observation, where the radiometer observes the atmosphere against the cold dark background of space. Fig. 1b shows a simulated line intensity profile for HCN (531.7 GHz) at two different altitudes over Titan and several mixing ratios (ratio of HCN to all gases). The 100 km lines are dominated by pressure broadening, the 500 km line is entirely Doppler broadened. In between, the line shape is a combination known as the Voigt profile. By examining these line profiles as a function of h_T, the minimum limb observation altitude, a model of the concentration/temperature/pressure profiles can be determined.

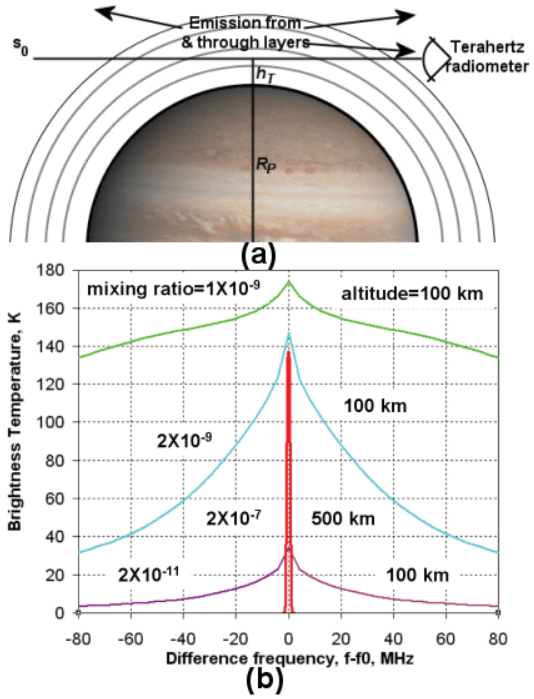

Fig. 1. (a) Limb sounding spectrometer configuration frequency. (b) A few spectral line profiles for HCN at Titan.

In order to retrieve separate the signal pressure profile from the concentration profile, it is necessary to observe more than one line of the relevant gas species. Because of the rapid movement of the spacecraft at Mars or Titan, the spectrometer needs to switch rapidly from one to the other while integrating the signal to produce near simultaneous measurements before the spacecraft motion degrades the measurement. Wind velocity determination uses the Doppler effect to determine the relative radial velocity between the spacecraft and the spot in the atmosphere being observed.

This paper examines the affect of system additive noise, phase noise, and line-to-line frequency switching on the quality of the measurement of the line profile and the line frequency accuracy.

II. System Additive Noise

The system under consideration is depicted in the block diagram of Fig. 2. The signal from the planet enters at the left, and is mixed in the mixer with a locally generated LO signal. The LO is derived from the ultra-stable oscillator (USO) primary frequency reference, and generated by a synthesizer at a frequency range around 30 GHz. From the synthesizer, the signal frequency is multiplied by the active millimetre wave/submillimeter wave chain by a factor of 18 to the signal frequency. The mixer IF output is amplified and converted to the range of 0-125 MHz, digitized, and analysed by an FFT-type discrete Fourier transform (DFT) spectrum analyser, followed by additional signal processing to be described later.

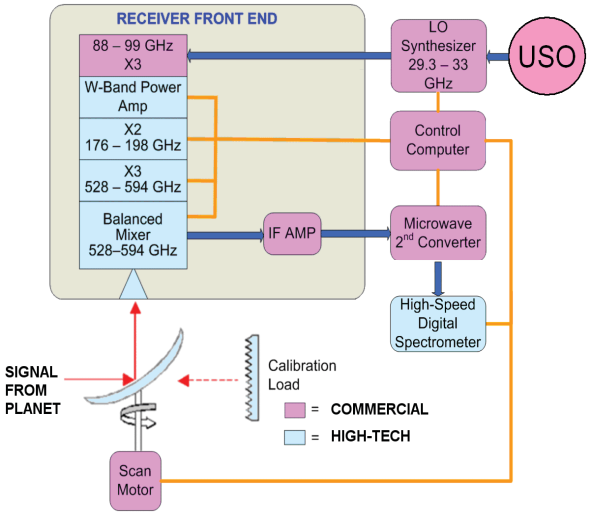

Fig. 2. Block diagram of spectrometer.

White noise from both the background of the observation and the mixer's thermal and shot noise enters the system, where it adds to the desired signal, resulting in measurement uncertainty. This additive noise affects both the frequency estimate and the amplitude profile determination of the spectral line.

A. *Effect of system noise on frequency estimate*

The effect of Gaussian additive noise on the frequency estimate of a single line (less than a channel bandwidth wide) has been analyzed by [1, 2] for the idealized case of an infinitely narrow sinusoidal CW line. The minimum possible frequency uncertainty, known as the Cramers-Rao lower bound (CRLB) [3] on the variance is given as:

$$\mathrm{var}\{\hat{\omega}_1\} = \frac{6\sigma^2}{\hat{A}^2 N\left(N^2-1\right)} \qquad \textbf{(1)}$$

$\hat{A}$ is the amplitude estimate, σ^2 is the Gaussian noise voltage variance, and N the total number of points in the measurement. In the nomenclature of [1], the frequencies are normalized to the inter-sample time, T:

$$\hat{\omega}_1 = 2\pi\hat{f}T$$

To express the frequency uncertainty in terms of the system temperature, T_{sys}, some identities must be used. The total noise power σ^2, is the product of the total noise power density, kT_{sys}, times the Nyquist bandwidth, $1/(2T)$, i.e.

$$\sigma^2 = \frac{kT_{sys}}{2T}\,. \qquad \textbf{(2)}$$

As for most spectrometers N^2>>1 so the CRLB frequency variance can be expressed as

$$\mathrm{var}\left\{\hat{f}\right\} = \frac{3kT_{sys}}{4\pi^2 N^3 T^3 \hat{A}^2}\,. \qquad \textbf{(3)}$$

For a DFT spectrometer, the channel bandwidth is the inverse of the total measurement time for each spectrum, $B_C = 1/(NT)$. In the measurement mode anticipated for the planetary spectrometer, successive measurements will have their power spectral densities summed [4]. Assuming these measurements are not correlated, frequency variance will be reduced the number of spectra averaged together, N_S. With this in mind, define the total integration time as:

$$\tau_I = N_S NT = \frac{N_S}{B_C} \qquad \textbf{(4)}$$

Finally the frequency uncertainty (deviation) is expressed as the square root of the variance,

$$\Delta f = \sqrt{\mathrm{var}\left\{\hat{f}\right\}} = \sqrt{\frac{3kT_{sys}B_C^2}{4\pi^2\hat{A}^2\tau_I}} = \sqrt{\frac{3B_C}{2\pi^2\tau_I}\frac{1}{SNR}}\,, \qquad \textbf{(5)}$$

where the last expression expresses the deviation in terms of the channel signal to noise ratio defined as the ratio of the line power ($\hat{A}^2/2$) to the channel noise power:

$$SNR = \frac{\hat{A}^2}{2kT_{sys}B_C} \qquad \textbf{(6)}$$

Usually the only variable than can be manipulated for any particular measurement is the integration time, the others being set by practical considerations.

B. *Effect of system noise on line profile estimate*

The total power in a "limited-bandwidth" channel is given by Rice (Dover, etc.), who derived it in the context of a band-limited square law device:

$$P = \sigma_C^2 + \frac{\hat{A}^2}{2}\,, \qquad \textbf{(7)}$$

which is the sum of the CW power and the channel noise power. The channel noise power, σ_C^2, is the total noise power σ^2 divided by the number of frequency channels:

$$\sigma_C^2 = \frac{\sigma^2}{N/2} = kT_{sys}B_C\,,$$

using the results from the previous section.

The variance of P [5, eq 4-16] is, again taking into account averaging over N_S records,

$$\mathrm{var}\{P\} = \frac{\sigma_C^2}{N_S}\left(\sigma_C^2 + \hat{A}^2\right). \qquad \textbf{(8)}$$

Note that if the channel contains pure noise, $\hat{A}$ =0 and the deviation for a single measurement (N_S=1) is 100% of the power, i.e. σ_C^2. On the other hand, if $\hat{A}^2 >> \sigma_C^2$, the deviation

is much higher, $\sigma_C \hat{A}$, since the power is the square of the sum of the line voltage and noise voltage. Expressing the channel power in terms of T_{sys} gives, for the power estimate deviation,

$$\Delta P \equiv \mathrm{dev}\{P\} = \sqrt{\mathrm{var}\{P\}} = \sqrt{\frac{kT_{sys}B_C}{N_S}\left(kT_{sys}B_C + \hat{A}^2\right)}. \quad \textbf{(9)}$$

For $\hat{A}$ ~0, the "signal" as well as the noise has a white spectrum, and it is sensible to define the power estimate deviation in terms of noise equivalent temperature difference:

$$\Delta P = k\Delta T_{eq} B_C$$

Putting this into (6) with $\hat{A}$ =0, and using (2) to replace N_S results in the radiometer equation:

$$\Delta T_{eq} = \frac{T_{sys}}{\sqrt{B_C \tau_I}} \quad \textbf{(10)}$$

Conversely, For $\hat{A}^2 >> \sigma_C^2$ it is more sensible to express the result as a relative power deviation,

$$\frac{\Delta P}{P} = \frac{2\sqrt{\mathrm{var}\{P\}}}{\hat{A}^2} = \sqrt{\frac{4kT_{sys}B_C}{N_S\hat{A}^2}} = \sqrt{\frac{2}{B_C\tau_I}\frac{1}{SNR}}, \quad \textbf{(11)}$$

with the last equivalence applying to the DFT spectrometer and including equations (4) and (6).

III. Phase Noise

In addition to the effect of AM noise on the frequency and line profile uncertainty, the effect of phase noise can be deteremined, in order to establish that the local oscillator

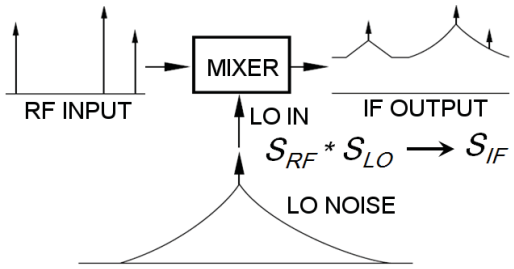

Fig. 3. LO Phase noise convolves with spectral lines to distort them.

does not degrade the measurement accuracy further. As depicted in Fig. 3, the LO phase noise profile is mixed with the input signal, polluting it. Since the mixer operates like a time domain multiplying element, the IF output is the product of the LO and RF signals in the time domain. Since the phase noise is described statistically in the frequency domain, the RF signal must be converted to frequency domain and, by the convolution theorem, the total signal is the convolution of the two. The phase-noise distorted IF signal is [3, p503] –

$$S_{IF}(f) = \int_{-\infty}^{\infty} S_{LO}(f - f')S_{RF}(f')df' \quad \textbf{(12)}$$

For example, if the LO were a perfect sinusoid at frequency F_{LO}, its Fourier transform would be $S_{LO}(f) = \delta(f + f_{LO}) + \delta(f - f_{LO})$ and the IF signal would simply be a phase shifted version of the RF and image.

One problem presented by the phase noise is distortion of the RF signal. If a strong line is close to a weak one, the phase noise will spread out the line, increasing the chance of it interfering with the weak one.

Besada [6] came up with a similar criterion based on an effective spectrometer channel filter. He noted that the output of one channel of the spectrometer would be:

$$S_{IF}(f) = |H(f)|^2 \int_{-\infty}^{\infty} S_{LO}(f - f')S_{RF}(f')df', \quad \textbf{(12a)}$$

similar to equation (12) but including the filter transmission function $H(f)$. The total channel output power is then given by an additional integration:

$$P = \int_{-\infty}^{\infty} |H(f)|^2 \left[\int_{-\infty}^{\infty} S_{LO}(f - f')S_{RF}(f')df'\right]df .$$

Now reverse the order of integration:

$$P = \int_{-\infty}^{\infty} S_{RF}(f') \left[\int_{-\infty}^{\infty} S_{LO}(f - f')|H(f)|^2 df\right]df'$$

which is a convolution of the RF signal with the IF channel response:

$$S_{CHAN}(f) = \int_{-\infty}^{\infty} S_{LO}(f - f')|H(f')|^2 df' . \quad \textbf{(13)}$$

This is just equation (12) substituting the RF line profile SRF with the channel profile, $|H(f)|^2$. Note that all of these spectral densities are two sided, integrated from –∞ to +∞. Hence, they should be determined from the normal one-sided density by dividing by two. Also, $S_{LO}(f)$ is assumed even in f.

The convolution of equation (13) can be used to calculate the distortion of the filter profile of the spectrometer channel, $|H(f)|^2$ in the output response, S_{CHAN} by the phase noise, S_{LO}. If S_{LO} were an ideal delta function S_{CHAN} would be the same as $|H(f)|^2$. In order to determine S_{LO} it is necessary to determine the effect of multiplication of the LO signal source up to the submillimetre wave signal frequency on the known (specified) low frequency LO source. According to the simple model proposed by Walls and DeMarchi [7, 8] the phase noise of a typical source can be divided into a central "carrier" where the carrier is sharply peaked at low Fourier frequencies < f_p, and the pedestal continues relatively flat out to some much higher frequency B. f_p might be around 1 kHz,

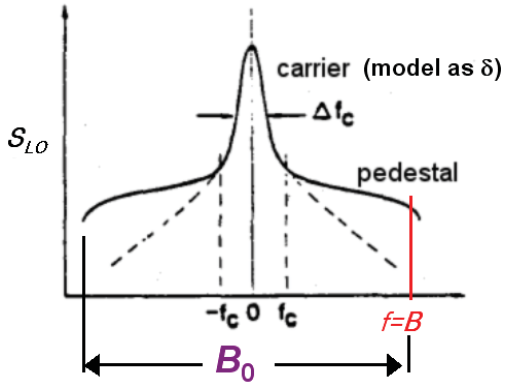

Fig. 4. LO phase noise spectrum, showing carrier in center and "pedestal". Based on [9].

B around 1000 kHz. See Fig. 4. As long as f_p is much smaller than the channel bandwidth (as in our case) the phase noise effect can be parameterized in terms of the total phase variance of the pedestal region, defined as:

$$\Phi_p = \int_0^{\infty} S_\phi^p(f)df , \quad \textbf{(14)}$$

where the parameter $\Phi_p \equiv \langle \phi_p^2 \rangle$ is the total integrated phase error in the pedestal and the sub- or superscript p refers to the pedestal. (Note that Walls and Dimarchi have the integration carried out from f_p, though Bava starts at 0. Since the pedestal has almost no power in the low-frequency-offset carrier region, the difference is inconsequential.)

Since multiplication into the submillimetre wave range by a factor of N increases the phase noise by N^2, the normal small angle approximation where $S_{LO} = S_\varphi$ is longer valid. Instead, the normalized carrier power (carrier power to total power) can be approximated:

$$P_c = \exp\left(-\Phi_p\right), \qquad \textbf{(15a)}$$

Then the normalized pedestal power is:

$$P_p = 1 - P_c = 1 - \exp\left(-\Phi_p\right). \qquad \textbf{(15b)}$$

At low phase noise levels ($\Phi_p << 1$) $P_c \approx 1$ and $P_p \approx \Phi_p$. As the phase noise levels increase with multiplication to higher frequencies, signal power is transferred from the carrier to the pedestal, broadening it. The model assumes that S_φ is not affected by multiplication, other than the general 20log$N$ increase:

$$S_\phi^p(f) = \frac{S_\phi^p(0)}{1+(f/B)^2} = \frac{2\Phi_p}{\pi B}\frac{1}{1+(f/B)^2}, \qquad \textbf{(16)}$$

assuming the pedestal exhibits a Lorentzian frequency dependence with 3-dB half-width bandwidth B, though exponents other than 2 could also be used.

To calculate the effect of phase noise on the power in the spectrometer channels, we want to determine S_{LO}. Walls and DeMarchi noted that the pedestal at frequencies well below its bandwidth followed a simple law:

$$S_{LO}^p(0) = \frac{2P_p^2}{\pi B \Phi_p}$$

Assume the pedestal has continues to exhibit a Lorentzian frequency profile at high phase noise levels with a two-sided bandwidth $\Delta\nu_p$, the complete power spectrum of the pedestal can be determined by combining the three previous equations and noting that S_{LO} integrated from 0 to ∞ gives the total pedestal power P_p:

$$S_{LO}^p(f) = \frac{2P_p^2}{\pi B \Phi_p}\left[\frac{1}{1+\left(2f/\Delta\nu_p\right)^2}\right] \qquad \textbf{(17)}$$

with the full-width bandwidth of:

$$\Delta\nu_p = 2B\frac{\Phi_p}{1-\exp\left(-\Phi_p\right)}$$

Note that for small values of the total phase error, Φ_p, $S_{LO} \rightarrow S_\varphi$, and $\Delta\nu_p \rightarrow 2B$. The model is valid until approximately half the average power *density* is in the pedestal so that

$$\exp\left(-\Phi_p\right) = \frac{\Delta\nu_p}{\Delta\nu_c}$$

where the carrier linewidth, $\Delta\nu_c$ is defined by [7, eqn (19)]:

$$\int_{\Delta\nu_c/2}^{\infty} S_\phi^c(f)\,df = \ln 2$$

More generally, if the carrier noise profile can be modelled as $S_\varphi(f) = K_{-\alpha} f^{-\alpha}$, where $K_{-\alpha}$ is determined from the magnitude of S_φ at some frequency then,

$$\Delta\nu_c = 2\left(\frac{\alpha-1}{\ln 2}K_{-\alpha}\right)^{1/(\alpha-1)}$$

A. *Effect of phase noise on spectrometer channel amplitudes*

Fig. 5(a) shows a generic frequency synthesizer phase noise spectrum S_φ at 30 GHz, as well as the frequency multiplied version at 540 GHz, with N=18. The pedestal S_{LO} is also shown. In addition, S_φ and pedestal S_{LO} for a synthesizer with 20 dB worse phase noise is shown (multiplied only) demonstrating the widened pedestal for Φ_p = 12. Shown in Fig. 5(b) are the dependencies on total phase error of the carrier power, pedestal power and S_{LO} pedestal bandwidth relative to S_φ pedestal bandwidth.

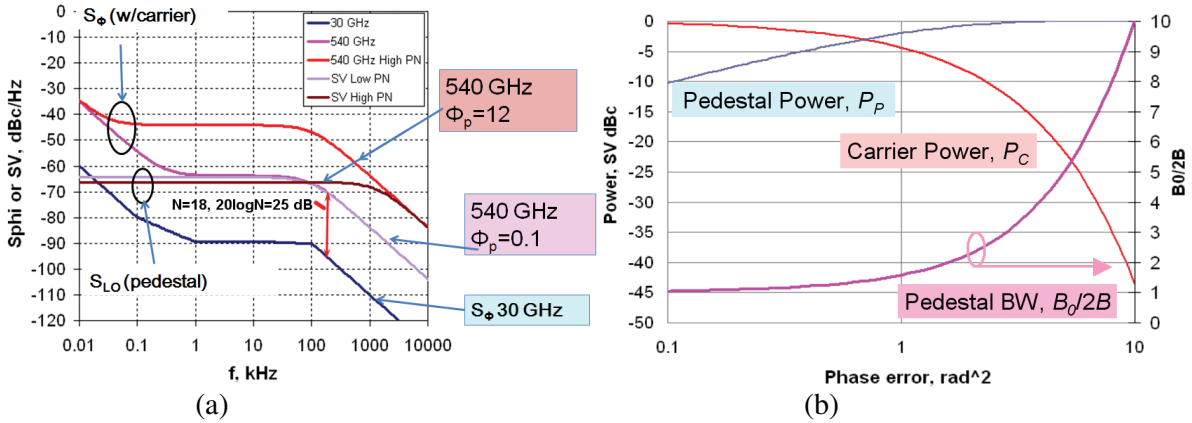

Fig. 5. (a) Synthesizer phase noise at 30 GHz compared to phase noise when multiplied to 540 GHz. For comparison, multiplied noise of a synthesizer with 20 dB more noise is shown. (b) Dependence of carrier power, pedestal power and pedestal bandwidth on phase error.

The results of the convolution calculation in equation (13) are shown in Fig. 6, demonstrating the distortion of the

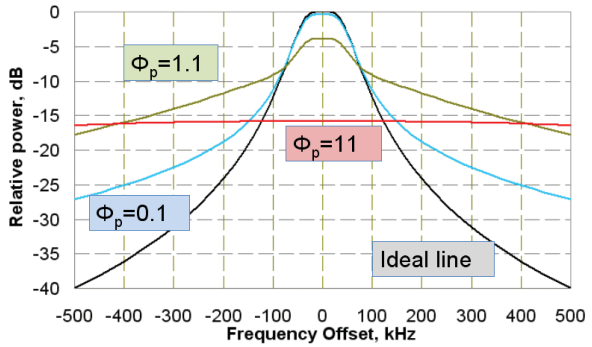

Fig. 6. Spectrometer profile distortion due to phase errors of 0.1, 1.1 and 11 rad^2 compared to the ideal line.

spectrometer line profile due to three levels of total phase error. The $\Phi_p = 0.1$ line is faithful to the ideal down to about -10 dB, but the $\Phi_p = 1.1$ line has leaked half the power of the channel into its neighbours. The $\Phi_p = 12$ profile is only barely recognizable as a channel filter response.

These results argue that that the phase error should be less than about 0.1 rad^2 to yield accurate line profiles.

A. *Effect of phase noise on frequency estimation*

To estimate the effect of phase noise on frequency measurement over some period of time, several frequency uncertainty measures can be used. One that is commonly adopted is the Allan or two-measurement variance, defined as:

$$\left(\frac{\Delta f}{\nu_0}\right)^2 \cong \sigma_y^2(\tau) = \frac{1}{2}\left\langle [\bar{y}_{k+1}(\tau) - \bar{y}_k(\tau)]^2 \right\rangle, \qquad \textbf{(18)}$$

where $\bar{y}_k(\tau) = \bar{\nu}_k / \bar{\nu}_0$ is the kth normalized frequency measurement averaged over time τ, and $\bar{\nu}_0$ is the frequency average over all measurements. Over long periods of time (tenths of seconds on up) the Allan variance can be determined from sequential time interval (phase) measurements. For shorter intervals, the Allan variance can be calculated directly from the phase noise spectrum [9]:

$$\sigma_y^2(\tau) = \frac{2}{(\pi\tau\nu_0)^2}\int_0^{f_h} S_\varphi(f)\sin^4(\pi\tau f)df$$
$$= \left(\frac{2}{\pi\tau\nu_0}\right)^2 \int_0^{f_h} \mathcal{L}(f)\sin^4(\pi\tau f)df \qquad \textbf{(19)}$$

In oscillator and synthesizer phase noise specifications and measurements, the phase noise density is often expressed using the symbol $\mathcal{L}$, to match what would be observed on a spectrum analyzer. Since S_φ includes the phase noise in both sidebands, $\mathcal{L} = S_\varphi/2$ [10]. To model the LO phase noise spectrum we break it into segments with fixed power frequency dependencies:

$$S_\varphi(f_{1,k} < f < f_{2,k}) = 2\mathcal{L}_k\left(\frac{f_k}{f}\right)^{\alpha_k} \qquad \textbf{(20)}$$

where $\mathcal{L}_k$ is the phase noise at a reference frequency f_k with a frequency dependence of $f^{-\alpha}$ over the frequency range stretching from $f_{1,k}$ to $f_{2,k}$. In the literature [9, 11] the values of the integral in equation (1b) are tabulated for single values of α assuming that they stretch from 0 to infinity. More complicated formulae can be derived for finite length segments, each segment having an Allan variance of:

$$\sigma_{y,\alpha}^2(\tau) = \frac{2}{(\pi\tau\nu_0)^2}\int_{f_1}^{f_2} 2\mathcal{L}(f_r)\left(\frac{f}{f_r}\right)^{\alpha}\sin^4(\pi\tau f)df$$

The oscillator phase noise spectrum can then be fit approximately by a piecewise $f^{-\alpha}$ series and integrated from 0 to some high frequency limit, f_h.

As an alternative, equation (19) can be integrated directly. However, at frequencies above $10/\tau$ or so, the sine factor in (19) oscillates so rapidly that it is difficult to integrate numerically. To solve this problem, the integral can be divided up in to a region with frequencies below $10/\tau$, integrated with the full integrand, and a region above $10/\tau$, where the oscillatory integrand is approximated by its average, 3/8.

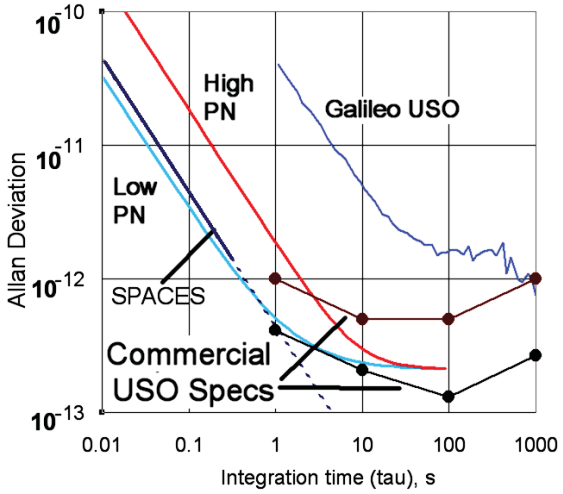

Fig. 7. Frequency Allan deviation due to high ($\Phi_p = 11$) and low ($\Phi_p = 0.1$) phase noise sources, compared to several USOs and the breadboard measurements.

Fig. 7 shows the result of the integration for two values of multiplied synthesizer phase error, 0.1 and 11 rad^2. For comparison some modern commercial USOs and the 1970s era Galileo-Jupiter USOs are also plotted. The broken trace labelled SPACES is calculated from the 540 GHz phase noise measurement on the breadboard spectrometer described later.

These numbers can be compared to the frequency accuracy required to achieve the desired wind velocity resolution. The Doppler relative frequency shift is the velocity divided by the speed of light, c, the velocity resolution ΔV is given by:

$$\Delta V = c\frac{\Delta f}{\nu_0}$$

For a typical desired wind velocity resolution of 3 m/s, the frequency must be accurate to 10^{-8}. Note that all traces in

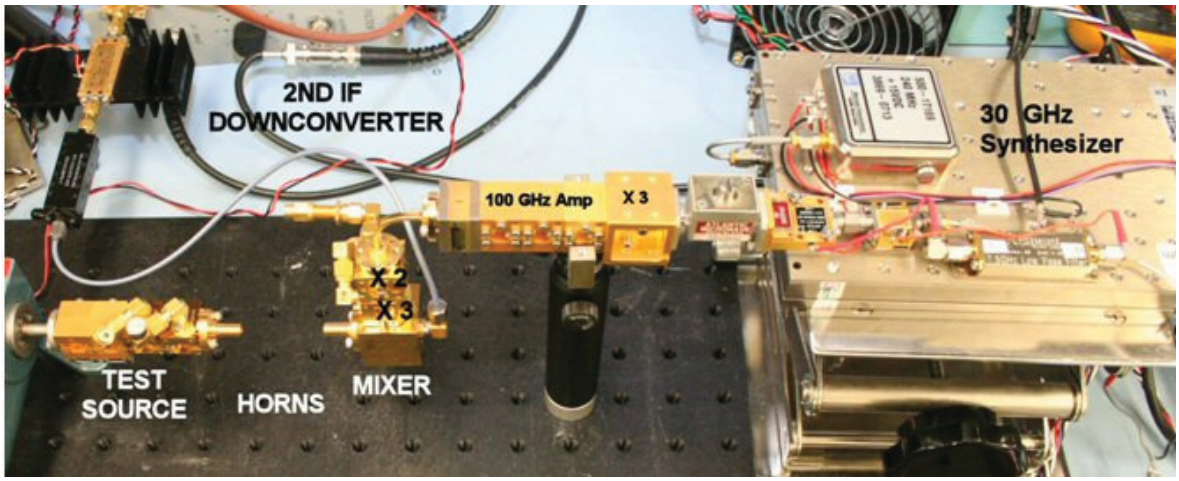

Fig. 8. Submillimeterwave Planetary Atmospheric Chemistry Exploration Sounder (SPACES) laboratory breadboard.

Fig. 7 are well below the range of 10^{-8} on these time scales. On longer time scales the frequency accuracy is dominated by the long term drift of the USOs. Over those time scales (years) other methods can be used to ensure that the USO frequency is determined and corrected for.

A synthesizer that satisfies the total phase error $\Phi_p < 0.1$ rad^2 requirement discussed earlier will meet frequency accuracy requirements of 10^{-8} as long as the measurement is made for longer than a millisecond or so.

One further point to note: the segment of the Allan deviation dominated by synthesizer phase noise ($\tau < 1$ second) has a $1/\tau$ integration time dependence, as opposed to the $\tau^{-1/2}$ dependence predicted by the white AM noise equation (5) presented earlier.

IV. Breadboard Measurements

To demonstrate that the planetary submillimetre wave spectrometer will work according to the requirements described above, a laboratory breadboard version has been built under a NASA Planetary Instrument Design and Development and Program contract. The breadboard is depicted in Fig. 8, which shows the synthesizer to the right, the front end multiplier chain and mixer in the middle facing the test source which made of an Agilent synthesized signal generator and sub millimeter chain at the middle left. Behind the test source is the 5 GHz IF second downconverter, which feeds a 0-125 MHz digitizer board that is part of the control computer, a standard PC to the right, out of the picture.

The digitization occurs at 250 Megasamples/second, and the spectra are generated by an FFT software algorithm, including a Hanning window to reduce side lobe generation. The LO synthesizer operates in the 30 GHz band, and is followed by an attenuator and a frequency tripler to raise the frequency to 100 GHz, where the signal is amplified to feed the X2X3 Schottky multiplier chain [12] to pump the mixer. The mixer is a balanced fundamental type [13, 14].

In these tests, the 540 GHz test signal is received at a frequency of 70 MHz. A single 4096-frequency spectrum using 32.8 μs of data and channel width of 30.5 kHz appears in Fig. 9. This is zoomed in to the region around 70 MHz, and it and the approximate signal-to-noise ratio of 20 dB is marked.

To assess the effect of switching frequencies rapidly, a continuous measurement was made for 6.3 seconds while switching LO frequencies approximately every 21 ms between 540 and 570 GHz, yielding 3.15 seconds of data for each frequency. In order to process these spectra, the line amplitude and frequency must be estimated from the FFT spectra.

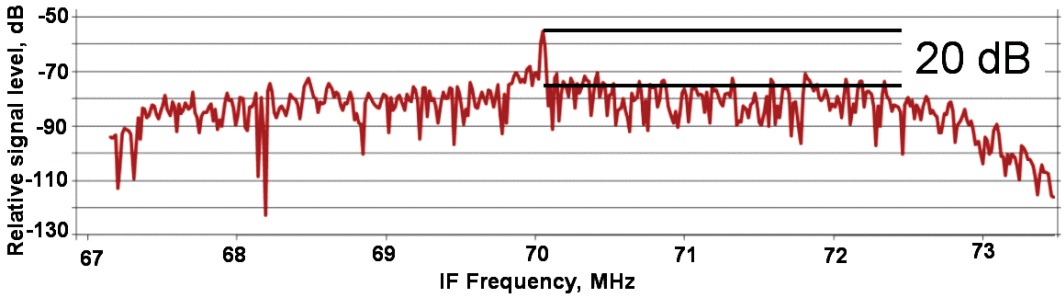

Fig. 9. A portion of a single spectrum showing the test signal at the 70 MHz 2n IF frequency.

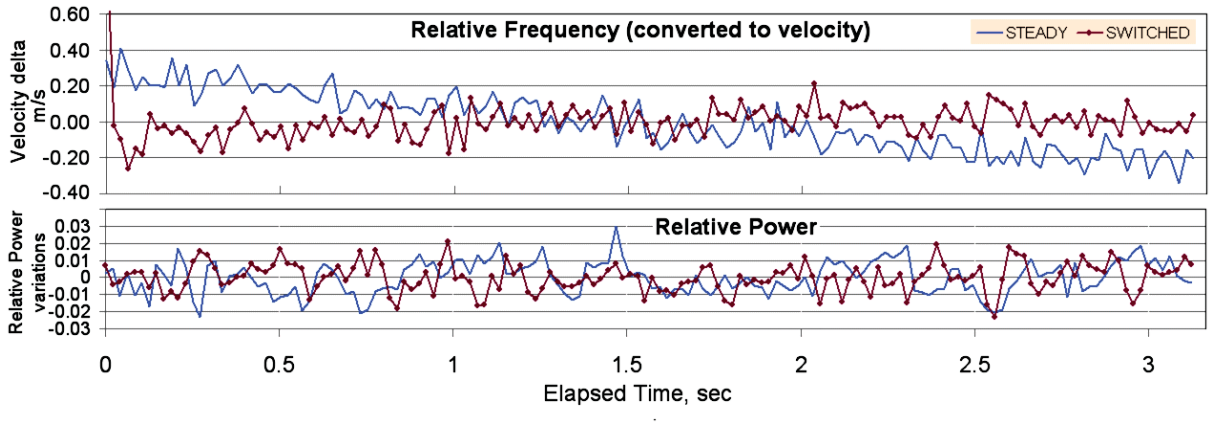

Fig. 10. Relative frequency (converted to velocity) and power plots over 3.15 seconds of observation.

A. *Frequency and channel power estimators*

In order to estimate the frequency and power in the CW test signal this an interpolation algorithm was used on the FFT data [15-17] starting with the amplitudes calculated from the spectrometer having N_C channels, $|X_k|$, k=1..N_C.

1. Find maximum magnitude peak, $|X_k|$, and the largest adjacent sample, $|X_{k+\alpha})|$, where $\alpha = \pm 1$.
2. Define: $\gamma = \left| \frac{X_{k+\alpha}}{X_k} \right|$
3. Calculate δ, the frequency offset from the center of the kth channel. For a DFT spectrometer with a Hanning window: $\delta = \alpha \frac{2\gamma - 1}{1+\gamma}$.
4. The frequency estimate is given by $f_T = (k+\delta)B_C$, where B_C is channel bandwidth.
5. For Hanning windowed data the amplitude estimate [15]:

$$X_T = \left| \frac{\pi\delta}{\sin \pi\delta} \right| \left(1 - \delta^2\right) |X_k|$$

A three-point interpolator calculated from the peak magnitude, $|X_k|$ and the two adjacent frequency magnitudes, $|X_{k-1}|$ and $|X_{k+1}|$ could be used [16, 18]. However, [17] notes that with reasonable SNR, this does not add substantially to the accuracy. The three-point interpolator was tried, but yielded results that differed by only a few percent from the two-point interpolator above.

B. *Measurement results*

Fig. 10 shows the 3.15 seconds of accumulated relative frequency and power data, comparing the switched data with a steady (unswitched) data set taken without changing LO frequency. For comparison to the 3 m/s velocity resolution requirement described earlier, the frequency data have been converted from frequency deviations to "velocity" deviations via multiplication by the speed of light, $3X10^8$ m/s. Each point is the average of the frequency (or power level) over the entire 18 ms record between switches. (The first 3 ms of data after each frequency switch is deleted to allow the synthesizer to settle on the new frequency).

Two things are apparent: first, there is a secular drift in both data sets, but more pronounced in the switched data. This is due to the unfortunate fact that the synthesizer has its own TCXO reference, and is not lockable to the main system reference as are the test generator and 5 GHz 2nd downconverter. As the synthesizer generates a fair amount of heat during the test, the lower amount of drift during the switched test is almost certainly due to the fact that the system stabilized during the steady test, which was performed directly preceding the switched test.

A second observation: other than the drift, there is no apparent difference between the steady and switched data.

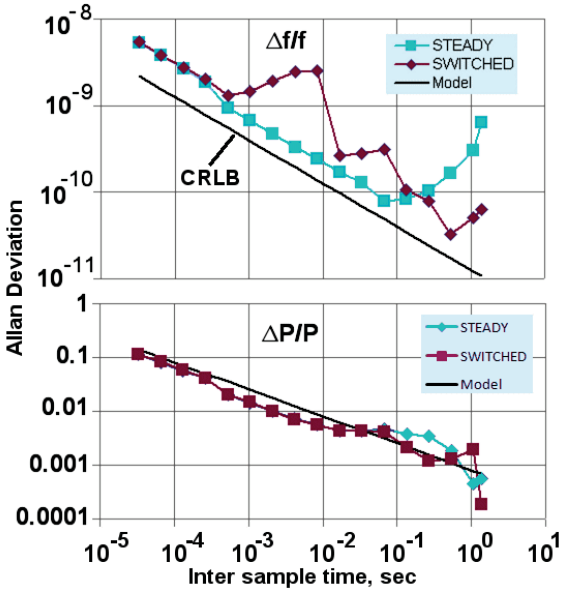

Fig. 11. Allan deviation comparison for frequency (top) and power (bottom).

The Allan deviation data depicted in Fig. 11 show a different story. As with the plots of Fig. 10, the relative power deviation shows very little difference between switched and steady data sets. However, the frequency deviation data show a large difference, especially in the

regime between about a half millisecond and 10-20 ms. A close up of the frequency deviation data during several switching sequences (Fig. 12) indicates the source of the problem. The frequency synthesizer requires longer than 2.5 ms to settle on the new frequency after switching, requiring about 10 ms instead. The original specification on the synthesizer was 100 ms. This variation would seem to compromise the use of frequency switching to accommodate the science requirements. However, the use of longer integration times between switching (100 ms) is acceptable (at Mars, at least), which eliminates the problem, as long as

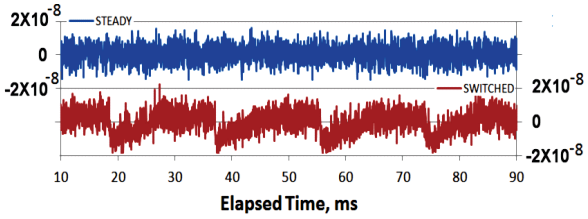

Fig. 12. Close up of frequency measurement over several switching cycles comparing steady and switched data.

the settling time is accounted for.

Plotted with the measured Allan deviation is the results of equations (5) and (11) earlier for the deviations due to system AM white noise, using BC=30.5 kHz and SNR=100 (20 dB). The fact that the dependence of the frequency deviation on time follows a $\tau^{-1/2}$ confirms the earlier prediction that frequency (and power) deviations are dominated by the AM white noise. The CRLB falls below the measurements, most likely because the simple DFT interpolation algorithm trades maximal likelihood estimation for speed and simplicity [17].

Finally, a phase noise measurement was made of the LO system, both at 30 GHz and 540 GHz. See Fig. 13. These are quick, somewhat rough measurements and should be considered uncalibrated, since the effect of the test oscillator has not been separated from that of the spectrometer. Nevertheless, the synthesizer measurement matches the specification (shown as diamonds) fairly closely. The calculated phase errors at 30 GHz and 540 from equation (15) are 0.00189 and 0.621 rad^2 respectively; the compare value at 540 GHz to the 30 GHz error multiplied by the square of the multiplication ratio: 0.00189 X 18^2 = 0.621, indicating model consistency.

V. Conclusions

Several key points about the submillimeter wave planetary atmospheric spectrometer have been demonstrated. The LO synthesizer total integrated phase noise error at the signal frequency should be < 0.1 radian^2. As long as this difficult to meet (considering lower power and mass demands) is met, the phase noise is much less critical to frequency accuracy for measurement times greater than about 1 millisecond. Likewise, USOs are stable ($\Delta f/f_0$<3X10^{-8}) for integration times of 0.1 sec or longer, but long term (10 years) stability is a problem that needs to be considered during mission planning. Finally, frequency switching works fine if the observation time is much longer than synthesizer settling time.

Acknowledgment

I would like to acknowledge the efforts of: Robert Lin for mixer and LO measurements; Pete Bruneau for machining the blocks; Mark Allen (Science Co-I) and Sam Gulkis for guidance on science requirements; John Gill and Choonsup Lee for device fabrication; Imran Mehdi, Peter Siegel as leaders of our team.

This work was performed at Jet Propulsion Laboratory/California Institute of Technology under contract to the National Aeronautics and Space Administration. © 2010 California Institute of Technology. Government sponsorship acknowledged.

References

[1] M.D. Macleod, "Fast Nearly ML Estimation of the Parameters of Real or Complex Single Tones or Resolved Multiple Tones," *IEEE Trans. Signal Processing*, pp 141-148, Vol. 46, No. 1, Jan. 1998.

[2] D. C. Rife, and R. R. Boorstyn, "Single tone parameter estimation from discrete-time observations," I*EEE Trans. Inform. Theory*, vol. IT-20, pp. 591-598, 1974.

[3] S. M. Kay. *Fundamentals of Statistical Signal Processing: Estimation Theory*, Prentice Hall, Englewood Cliffs, NJ, 1993.

[4] W.H. Press, S. A Teukolsky, W.T. Vetterling, B.P. Flannery, *Numerical Recipes in C++*, Cambridge University Press, Cambridge, 2002.

[5] S.O. Rice, "Mathematical analysis of random noise," Bell System Tech. J., Vols. 23, 24, reprinted in *Selected Papers on Noise and Stochastic Processes*, ed. Nelson Wax, Dover, New York, 1954.

[6] J.L. Besada, "Influence of local oscillator phase noise on the resolution of millimeter-wave spectral-line radiometers," *IEEE Trans. Instrum. Meas*., IM-28, no. 2, June 1979.

[7] F.L. Walls and A. DeMarchi, "RF Spectrum of a Signal after Frequency Multiplication; Measurement and Comparison with a Simple Calculation," *IEEE Trans. Instrum. Meas*., IM-24, no. 3, Sept. 1975.

[8] E. Bava, A. DeMarchi, A. Godone, "Spectral analysis of synthesized signals in the mm wavelength," *IEEE Trans. Instrum. Meas*., IM-26, no. 2, June 1977.

[9] S.R. Stein, "Frequency and Time – Their Measurement and Characterization," Ch. 12 of *Precision Frequency Control*, Vol. 2, edited by E.A. Gerber and A. Ballato pp. 191-416, Academic Press, New York, 1985.

[10] D. Allan, H. Hellwig, P. Kartaschoff, J. Vanier, J. Vig, G.M.R. Winkler, and N.F. Yannoni, "Standard terminology for fundamental frequency and time metrology," *Proceed. 42nd Annual Freq. Control Symp*., 1988.

[11] J.A. Barnes et al, "Characterization of frequency stability, *IEEE Trans. Instrum. Meas*., IM-20, no. 2, May 1971.

[12] A. Maestrini, J. Ward, J. Gill, H. Javadi, E. Schlecht, C. Tripon-Canseliet, G. Chattopadhyay and I. Mehdi, "A 540-640 GHz High Efficiency Four Anode Frequency Tripler," *IEEE Trans. Microwave Theory Tech*, Vol. 53, pp. 2835–2843, Sept. 2005.

[13] E. Schlecht, J. Gill, R. Dengler, R. Lin, R. Tsang, and I. Mehdi, "First wideband 520-590 GHz balanced fundamental Schottky mixer," presented at the Eighteenth International Symposium on Space Terahertz Technology, Pasadena, CA, Mar. 2007, available at http://www.nrao.edu/meetings/isstt/papers/2007/2007296000.pdf

[14] E.T. Schlecht, J.J. Gill, R.H. Lin, R.J. Dengle, and I. Mehdi, "A 520-590 GHz Crossbar Balanced Fundamental Schottky Mixer," to be published in *IEEE Microw. Wireless Compon. Lett.*

[15] T. Grandke, "Interpolation algorithms for discrete fourier transforms of weighted signals," *IEEE Trans. Instrumentation and Measurement*, Vol. IM-32, pp 350-355, June 1983.

[16] J. Schoukens, R. Pintelon, and H. Van hamme, "The interpolated fast fourier transform: a comparative study," *IEEE Trans. Instrumentation and Measurement*, Vol. 41, No. 2, pp 226-232, June 1983.

[17] I. Santamaria, C. Pantaleon and J. Ibanez, "A comparative study of high-accuracy frequency estimation methods," *Mechanical Systems and Signal Processing* Vol. 14, No. 5, pp 819-834, 2000.

[18] [18] D.C. Rife and G.A. Vincent, "Use of the discrete Fourier transform in the measurement of frequencies and levels of tones," *Bell Syst. Tech. J*., vol. 49, pp. 197-228, Feb. 1970.